Unintended consequences: why carbonation can dominate in microscale hydration of calcium silicates

N. Ferralis[1,*], D. Jagannathan[1,*], J.C. Grossman[1], K.J. Van Vliet[1]

[1]*Department of Materials Science and Engineering, Massachusetts Institute of Technology, Cambridge, Massachusetts, 02139 USA*
** These authors equally contributed to this work.*

Supplementary Information

S.1 Picoliter confined hydration droplet

Figure S.1 shows the experimental setup used to create supersaturated confined volumes for the growth of hydration and carbonation of tricalcium silicate products. A key component of these experiments is the creation of picoliter droplets of aqueous fluids achieved using a microinjector (Femtojet, Eppendorf-Nethler-Hinz, GmbH Hamburg, Germany). These microinjectors are connected to microcapillaries (Femtotip, Eppendorf-Nethler-Hinz, GmbH Hamburg, Germany) that deliver picoliter droplets of fluid upon controlled application of pressure. Arrays of independent confined reaction environments are achieved using a joystick-controlled micromanipulator that enables lateral sample translation of the microcapillary. The reaction between cement clinker (specifically, tricalcium silicate) particles and aqueous fluids, both deposited on the glass slide, is observed through an inverted optical microscope (Olympus America Inc, Chelmsford MA, using a 20X objective). Optical micrographs are collected fusing a 5.5 megapixel CMOS camera (Andor Technology PLC, Belfast, Ireland), connected to a workstation for local image storage and systematic analysis.

Figure S.1 Experimental setup. Picoliter droplets of aqueous media are delivered using microcapillaries (a) regulated by microinjectors (b). Micromanipulator (c) controlled by joystick (d) enables 3D motion of the microcapillary. The hydration reaction as it unfolds on the glass slide (e) can be observed through the optical microscope (f). Camera attachment of the optical microscope enables storing and subsequent analysis of images on a local computer.

Droplet synthesis Confined reaction volumes with few, controllable, nucleation events were created at room temperature with the following protocol. A suspension of monoclinic tricalcium silicate, Ca_3SiO_5 (termed C_3S in cement chemistry notation, with 45 μm fineness; W. R. Grace & Company), was obtained by dissolving 10 g in 50 mL of isopropanol in a plastic centrifuge tube. Immediately before an experiment, the content in the tube were perturbed by manual shaking and allowed to settle until a section of translucent supernatant develops. The tube was agitated lightly enough that the supernatant became opaque, but not vigorously enough to disturb the C_3S residue at the bottom of the tube. As the particles resettled, transparent, translucent and opaque sections develop in the supernatant. Approximately $\sim$ 50 μl sample was drawn from the translucent section (red in Figure S.2) of the supernatant to deposit on the glass coverslip. When the isopropanol evaporates, an irregularly shaped deposit of microscopic tricalcium silicate particles remained on the glass slide. Empirically, we found that samples of suspension (that will be deposited on the

glass slide) drawn either from the fully transparent or opaque sections of the supernatant resulted in a distribution of clinker particles that is too sparse or too dense, respectively. In the latter case, clinker particles can agglomerate to form clusters (Figure S.2), defeating the purpose of these experiments to access the reaction interface between cement clinker particles and aqueous media. A 100 μL volume of inert paraffin oil was drawn into a pipette to cover this deposit of tricalcium silicate particles on the glass slide. We gently brought the microcapillary in contact with the surface of the glass slide beneath the droplet of oil. We then created sequences of picoliter droplets of aqueous media (degassed in vacuum of 29" Hg for ∼3 hours) with diameter ∼ 50μm (see Figure S.3a). We explored three alternatives for hydrating aqueous media: water, NaOH solution (pH 12), and saturated solution of $Ca(OH)_2$.

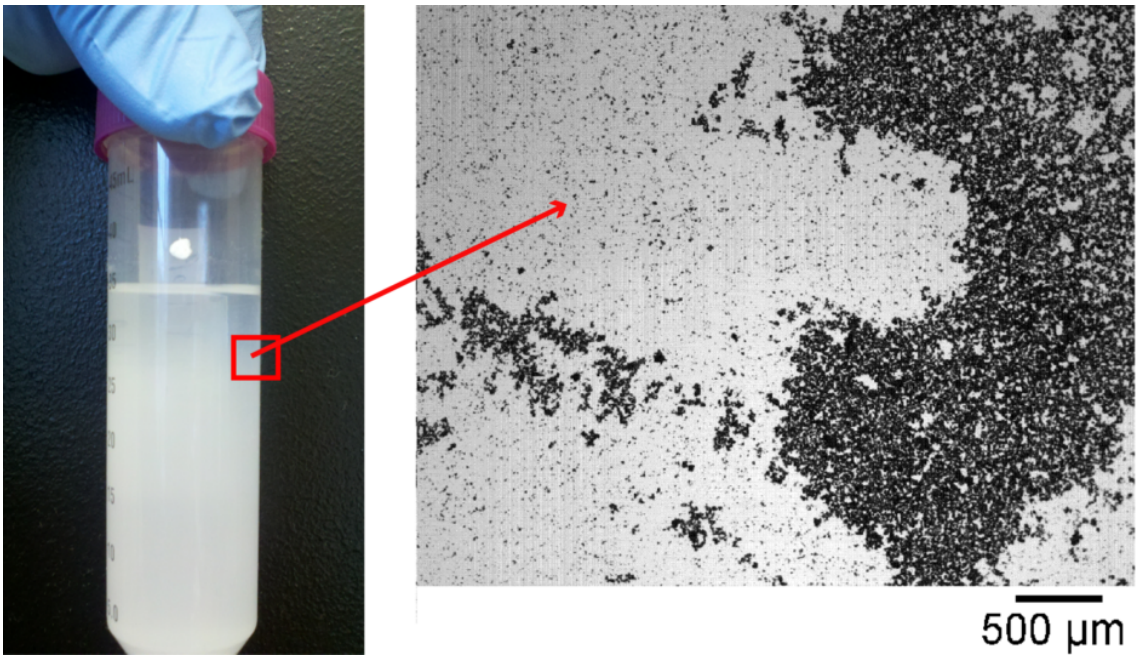

Figure S.2 (Left) Supernatant suspension of tricalcium silicate in isopropanol after agitation and decantation. The translucent supernatant is shown within the red square. (Right) Translucent supernatant (Approximately ∼ 50 μ) is deposited on a glass coverslip, with optimal dispersion.

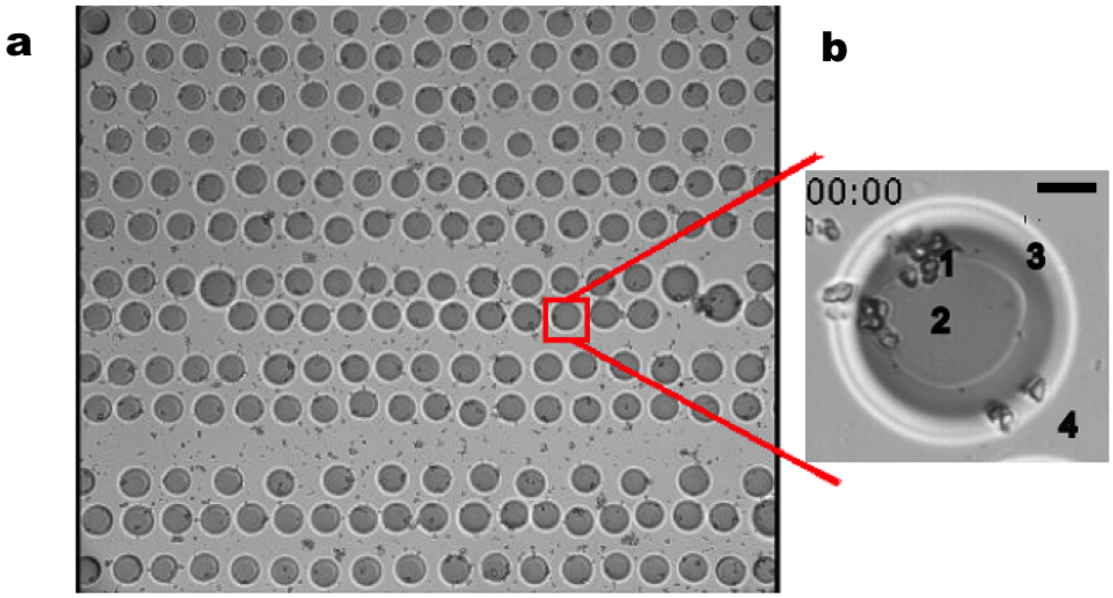

Figure S.3 (a) Array of picoliter droplets of NaOH pH 12 reacting with microscopic tricalcium silicate particles deposited on a glass slide observed under optical microscope. (b) Close-up view of one of the droplets at start of the experiment (time 00:00h, scale bar: 10 μm) with tricalcium silicate particles (1) at the periphery of the droplet of aqueous media (2). tricalcium silicate particles are also seen on the oil-water interface (3) and outside the droplet (4) in contact with oil. These particles do not undergo any reaction.

S.2 Reaction interface growth rates within droplets

The magnification provided by the optical microscope (objective: 20X) combined with the resolution of the CMOS camera, resulted in a spatial resolution of 0.3 μm/pixel. Reaction growth rates of the reaction interfaces within the droplet were measured using Cell Profiler ^{TM} [1] (Figure S.4a). We used the tracking module to compute the velocity (growth rate) of the reaction interface. The efficient use of tracking module required the tracked object (the reaction interface in this case) to be starkly distinct from the background. We achieved this contrast by subtracting the image at timestep $n-1$ from the image at timestep n, where a unit time step corresponds to 20 min. We found 20 min to be the smallest unit time step that produced detectable edges of the interface after the subtraction process. Time, t = 0, was chosen to denote the point in time when the reaction product became detectable at the scale of our observation ($\sim$ μm). The results of this process are shown in Figure S.4b. This process produced a sequence of images in which we can clearly contrast a white moving edge of the interface from the dark background. This sequence of images served as an input to the tracking module which then extracted the coordinates of the centroid of the moving edge as a function of time. Thus, time dependent growth rate was calculated as distance travelled between subsequent time steps (from coordinates of the centroid of the edge of the interface at times n and $n-1$) divided by unit time step (20 min). It is likely that the growing product adopted the symmetry of the space into which it is growing.

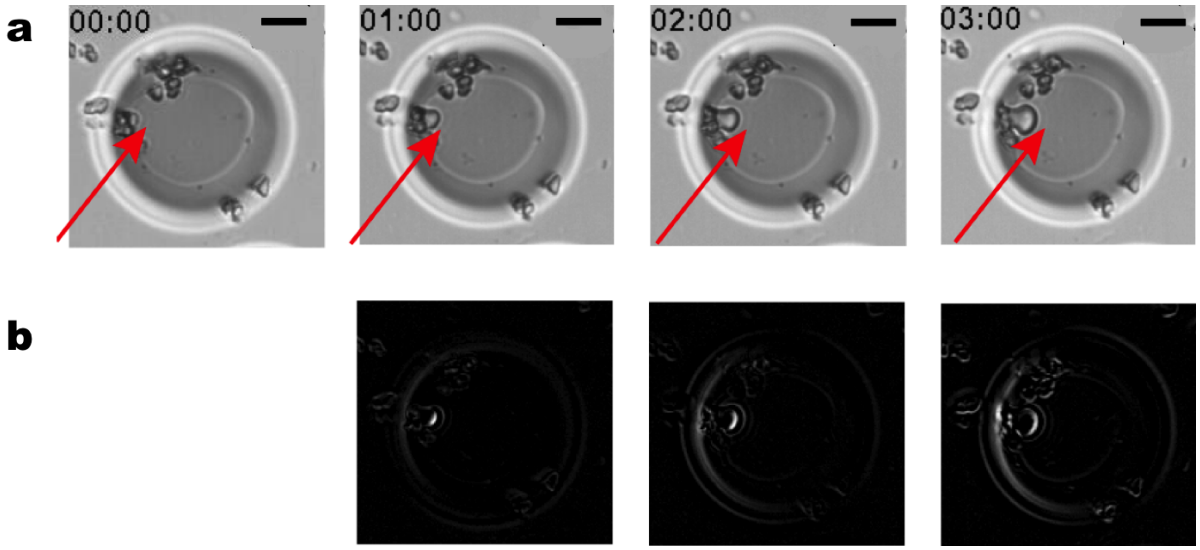

Figure S.4 (a) Dynamics of the reaction interface (red arrow points to leading edge of the interface) at 0, 1, 2, and 3 h. (b) Sequential image subtraction at time n from that at time $n-1$, $n \geq 1$ enabled high-contrast tracking of the interface and centroid that quantifies the rate of growth. (Scale bar: 10 μm)

We calculated growth rates of the interface that extended from reacting tricalcium silicate particles within these oil-confined picoliter aqueous droplets. The growth rates (Fig. S5) were calculated for tricalcium silicate particles reacting with droplets containing NaOH and at pH 12, and ranged from 0.05 to 1.5 μm/h with a mean +/- standard deviation of 0.77 +/- 0.25 μm/h. which are of the same order of magnitude as 0.1 um/hr calculated by [2] for wetting of a tricalcium silicate pellet imaged via atomic force microscopy [2]. Our measured growth rate of the initial, radially extending interfaces compares well with that calculated by Ref. [2] up until the morphology of the hydration product changed. To illustrate hydration product with "flat" morphology (and hence presumably constant growth rate), Ref. [2] included an AFM image taken at $t = 4$ h. Thus, we infer that the hydration product they observe exhibited a constant growth rate and flat interface for at least 4 h.

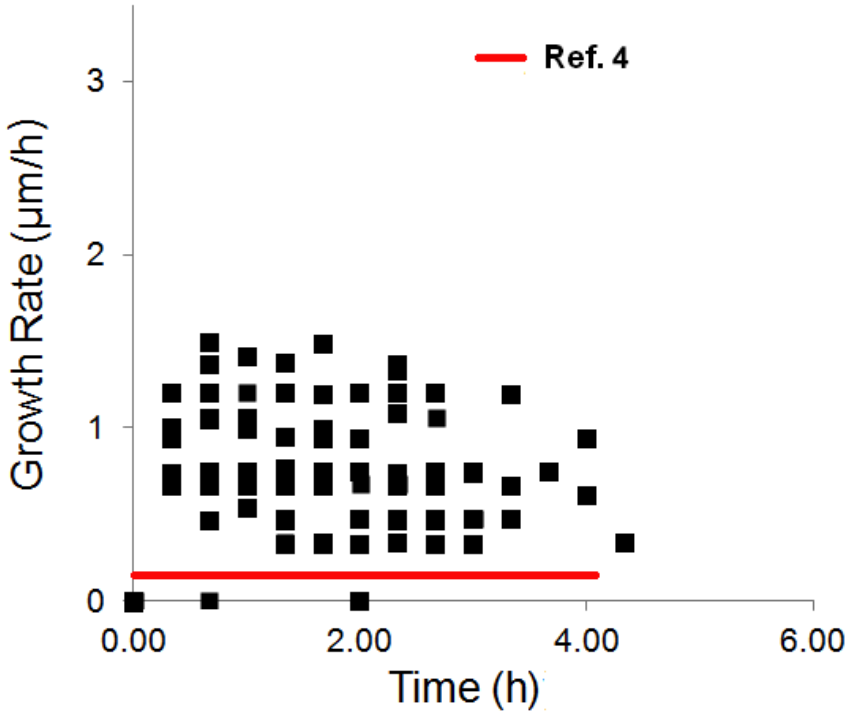

Figure S.5 Growth rates of hydration product computed by tracking growth fronts of 30 interfaces using image analysis algorithms described in the main text. Calcium trisilicate particles are reacting with aqueous droplets containing NaOH and at pH 12.

Our quantitative results on the growth rate of interface up until this growth front transition are consistent with lack of diffusion control in the initial stages of growth. Figure S.5 shows the results of our image analysis. We report growth rates of the interface up only within the interface-limited growth regime (and the growth front remains arc-like). We find average growth rates of $\sim$0.5 µm/h.

Effect of spatial distribution of calcium silicate particles on growth rates The differing spatial distribution of calcium silicate particles in each droplet did not have detectable effects on the growth rate of the product interface, within the instrumental resolution. It is important to note that the instrumental resolution is similar to the scale of the growth, and therefore the error could be of the same order of magnitude of the measured growth rates. In our limiting case, we can assert that the clinker particle distribution within/around the droplet influences the growth rate of the product interface within an order of magnitude. We note that our growth rates are the same order of magnitude as that reported in Ref. [2] for a flat growth front. We also note that the growth rates are relatively constant over the measured time periods. If the reaction were controlled by diffusion, the average growth rate at $t = 2$ h would be 4 times lesser than that at $t = 1$ h, that at $t = 3$ h would be 9 times lesser, and so on. Since we do not observe such a drastic decay of growth rates,

we further confirm that the growth kinetics is interfacially-driven.

The authors of that study do not confirm the chemical identity of the hydration product. However, they report that this hydration product grows by the aggregation of nanoparticles [2] (resolved using AFM to have dimensions of around 1000 nm^3).

S.3 Interfacial reaction growth kinetics

This surface nature of carbonation reactions (as opposed to the bulk nature of hydration reactions) is determined by the Fickian diffusion of CO_2 through from the paste surface into the bulk [3]. Therefore the diffusion-limited rate of carbonation is mainly responsible for the confinement of a carbonated surface layer, while minimal carbonation is expected and observed within the bulk. The rate of carbonation in macroscopic pastes can also be accelerated or artificially induced by increasing the CO_2 concentration, as well as by changing the Ca^{2+} supersaturation through different humidity conditions [4,5]. For quasi-two-dimensional (2D) systems, growth kinetics (and spreading) of mobile species from a reservoir over a flat surface are usually driven by diffusion, through wetting. Under the assumption that the spreading front from the nucleation site is circular or arc-like (with radius R), the atomic and molecular mobility on top of the surface is granted by the availability of such atoms/molecules from the reservoir. As the front grows, coverage is proportional to the area of the circular sector. Conceptually, as the front grows, the reservoir must be able to supply material to the front and the diffusion velocity from the reservoir to the front is the limiting factor. In pure 2D-diffusive systems, the front progression time t is proportional to R^2. For three-dimensional (3D) spherical growth, the front progression time t is proportional to the volume of the spherical sector, and therefore to R^3. For systems with more complex geometries (e.g., annular disks), the time dependence is $t \propto R^\beta$ ($\beta \geq 2$). For diffusion-limited systems, this dependence equates to $R \propto t^\alpha$ ($\alpha \leq 0.5$) [6,7]. For interface-limited systems, diffusion is such that the supply of mobile atoms to the growing front is constant, and therefore the concentration of mobile species at the reservoir and at the front is constant. The limiting factor is the series of processes, chemical reactions, and surface interactions that take place at the interface at the front [6,7]. The growth rate of the interface is therefore solely proportional to the extent of the interface itself, and therefore the growth time is proportional to the perimeter of the growth front (and so to its radius, R). The relation $R(t)$ is therefore linear.

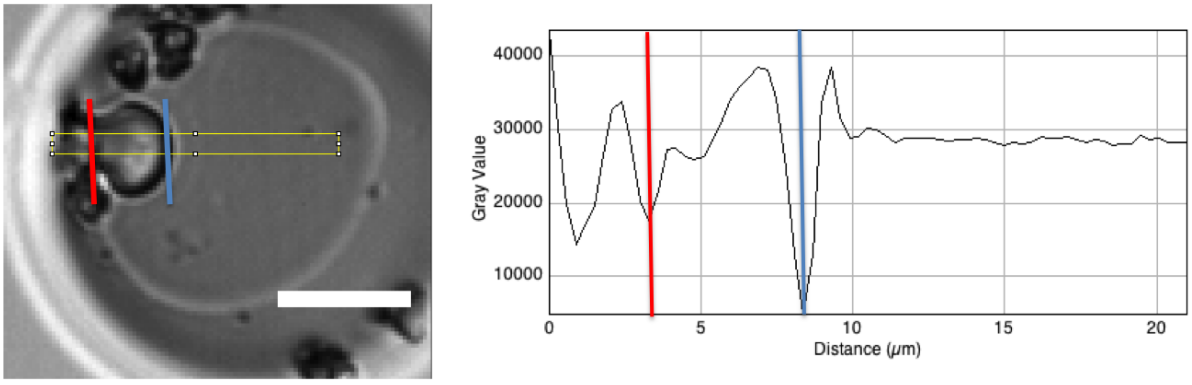

Figure S.6 Growth kinetics within a single droplet is measured from the optical images (scale bar: 10 μm), by integrated line profiles over the growing reaction product (as described in main text). The front edge of the reaction byproduct is highlighted in blue over the minimum of the profile. The tricalcium silicate particle is identified in the local minima highlighted by the red line.

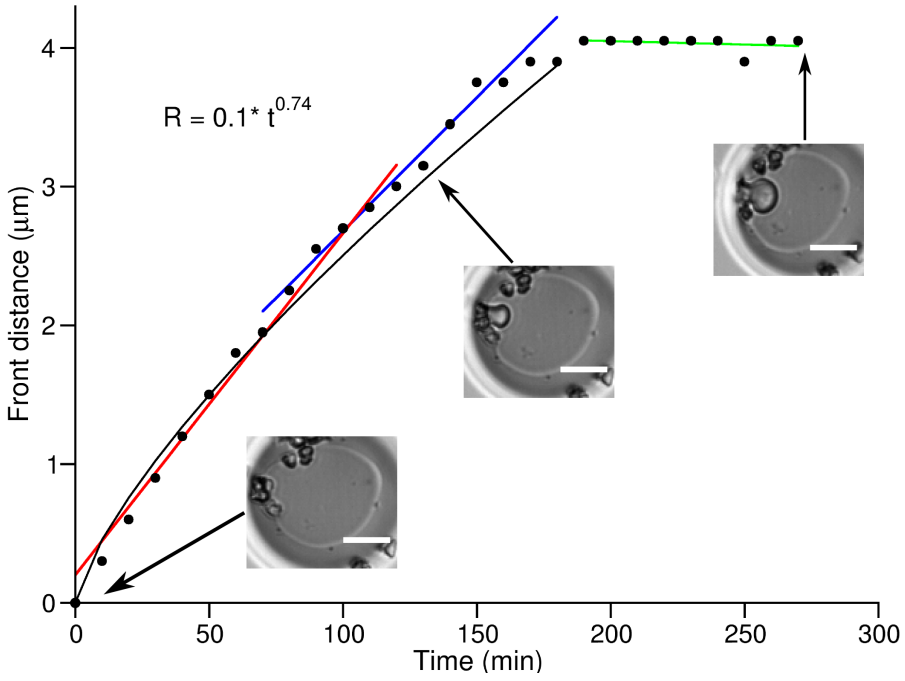

Figure S.7 Typical evolution kinetics of the growth profile measured from the C_3S particle. Growth and consolidation regimes are distinctively visible. Growth regimes follow power laws (black line) indicating an interface-driven growth mechanism, and within itself it can undergo different linear growth regimes (red and blue lines). During the consolidation regime, growth ends or it is significantly slower, indicating a diffusion-limited regime (green line). The images corresponding to the initial, intermediate and final growth stages are shown (scale bar: 10 μm).

Quantification of the growth kinetics in picoliter droplets Growth kinetics were analyzed by tracking the distance between the front of the growth product (carbonate, as confirmed by Raman spectroscopy) formation from the microparticle, through integrated line profiles (Figure S.6) via image processing software and analysis (ImageJ [8,9]). The image was oriented such that the growth direction of the reaction byproduct was horizontal. Therefore, the radius R of the arc-like front was measured by counting the number of pixels between the growing front and the C_3S particle, following a conversion through the image resolution. For each reactive particles analyzed, growth kinetics was extracted through a power-law fit ($R = A * t^B$), or by piecewise linear fits across different time ranges. Typical growth kinetics curves acquired from the C_3S particles in picoliter-volume droplets are depicted in Fig. 1b of the main text and Fig. S.7). The growth trend can be divided in two main regions: growth and consolidation. Growth regimes follow power laws with an exponent that is α >0.5 for every particle analyzed. This indicates that the growth kinetics is dominated by interface-driven growth mechanisms, as previously noted. (However, previous work has without proof attributed this growth reaction chemistry to hydration [2], rather than carbonation as shown in this work.) The mobile species are Ca^{2+} ions dissolved from the C_3S particle. This particle acts as a reservoir of Ca^{2+} ions, and the cation diffusion to the front is responsible for both nucleation at and subsequent growth of the carbonate away from the C_3S particle surface. While a reaction completely driven by interfacial processes would follow a linear trend, a very slow change in diffusivity of Ca^{2+} ions during the growth regime is responsible for an evolution that follows a power law with an exponent α between 0.7 and 0.9, rather than a linear trend. Furthermore, subregions of linear growth (red and blue linear fits in Figure S.7) can be observed, and the change in growth rate is directly attributed to the change in diffusivity. The small change in diffusivity of Ca^{2+} may be due to partial dissolution of the initial C_3S particle.

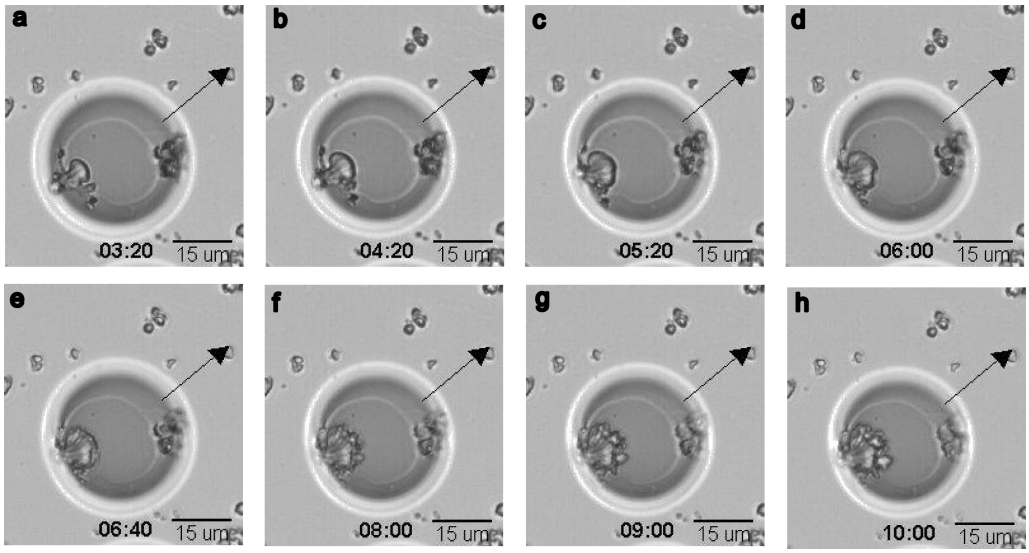

Figure S.8 Morphological evolution of the growth of reaction byproducts. The transition from Interface-limited growth (a-c) to diffusion limited growth (d-h) leads to the formation of dendrites. The arrow indicates the direction of growth, and time is indicated in hours:min.

A transition from interface-limited to diffusion-limited growth is observed when the growth ends or is severely retarded (green line in Figure S.7). The combination of C_3S depletion and water evaporation may ultimately reduce the available diffusive Ca^{2+} ions. Under this regime, the growth – if persistent – continues in a morphologically distorted growth front, typically through the formation of dendrites (Figure S.8) enabled by dissolved Ca^{2+} ions from the adjacent solution.

S.4 Mechanisms of accelerated C-S-H nucleation in C_3S via $CaCl_2$

$CaCl_2$ is a known reaction accelerator at the micro- to macroscales [10,11], but the mechanism by which this species enables a faster hydration rate has not been proven conclusively [10]. Based on x-ray microscopy studies of C_3S suspensions in $CaCl_2$ solution, Juenger *et al.* proposed that C-S-H was the reaction product formed in the early stages of hydration around the C_3S particle, and was more porous than that formed in conditions lacking $CaCl_2$; they posited that increased porosity enabled faster diffusion of water and calcium and silicate ions and, thus, higher growth rates of C-S-H [10]. On the other hand, Thomas *et al.*, based on modeling of experimental data from calorimetric experiments, proposed that $CaCl_2$ would influence the nucleation of C-S-H but would not affect the growth rate of C-S-H [12].

S.5 Cement paste preparation

Cement pastes were prepared at room temperature according to the following protocol. Five g of monoclinic tricalcium silicate (C_3S) were added to a glass vial with 2.5 g of aqueous media (water/solid ratio of 0.5) and mixed the contents using a stirrer for 5 mins. Approximately 0.5 g of the wet paste was transferred onto a glass slide using a spatula. Samples in which evaporation of aqueous media was not controlled were allowed to hydrate while exposed to ambient atmosphere. Other samples were sealed in a petri dish partially filled with deionized water so as to create an atmosphere of high relative humidity. Inside the Petri dishes, glass slides were secured on an elevated platform so as to avoid direct contact with a surrounding pool of water. This design does not fully prevent evaporation of aqueous media. Therefore, we further characterized areas of cement paste least susceptible to evaporation, i.e. the surface of the cement paste in contact with the glass slide. We label this surface as the "bulk" of the cement paste in the main text. After preparation, samples were exposed to the normal atmosphere only during the Raman spectroscopy experiments and were discarded afterwards.

S.6 Carbonation reactions during calcium trisilicate hydration

In absence of carbon dioxide, calcium trisilicate hydration is based on the reaction [11]:

$$C_3S + 3H_2O \rightarrow 3Ca^{2+} + H_2SiO_4^{2-} + 4OH^-$$

In presence of atmospheric carbon dioxide, this is dissolved in water to form carbonic acid [13]:

$$CO_2(g) + H_2O = H_2CO_3^*$$

$$H_2CO_3^* = H_2CO_3$$

Dissociation of carbonic acid leads to the formation of bicarbonate and carbonate ions:

$$H_2CO_3 = H^+ + HCO_3^{-1}$$

$$HCO_3^{-1} = H^+ + CO_3^{-2}$$

Formation of solid calcium carbonates results from the reaction of free Ca^{2+} ions (from the dissolution of calcium trisilicate and calcium hydroxide [13]) and CO_3^{-2} carbonate ions:

$$Ca^{2+} + CO_3^{-2} = CaCO_3(s)$$

S.7 Effects of hydration time scales on "surface" carbonation

As the time-scale of carbonation (and its effects on hydration) depends strongly on the length scale, it is important to reconcile surface phenomena with the expected and observed later stages of bulk hydration. At later stages of hydration ($\sim$1 day to 1 week), the presence of carbonates in cement pastes was seen as less pronounced. Figure S.9 shows Raman spectra for pastes maintained at high relative humidity atmospheres, minimizing evaporation of aqueous media while not changing exposure to CO_2 in the air. These spectra exhibited carbonate peaks at 2–4 days hydration that were reduced relative to those in Figs. 3 and 4a-b; significant levels of carbonation were observed only after 14 days. Under these conditions, the aqueous medium is consumed in the formation of $Ca(OH)_2$ and C-S-H, such that carbonation then takes place through reaction of these products directly with CO_2 in the atmosphere. For a given surface area of such porous reacting materials, moist pastes (hydrated one day or less) would then form calcium carbonates at the surface faster than pastes hydrated for a few days or more. This rate difference is attributable to the relative competition between water evaporation (resulting in carbonation for short hydration times) and carbonation (directly via the gaseous atmospheric CO_2 at long hydration times), as depicted in Fig. 4d.

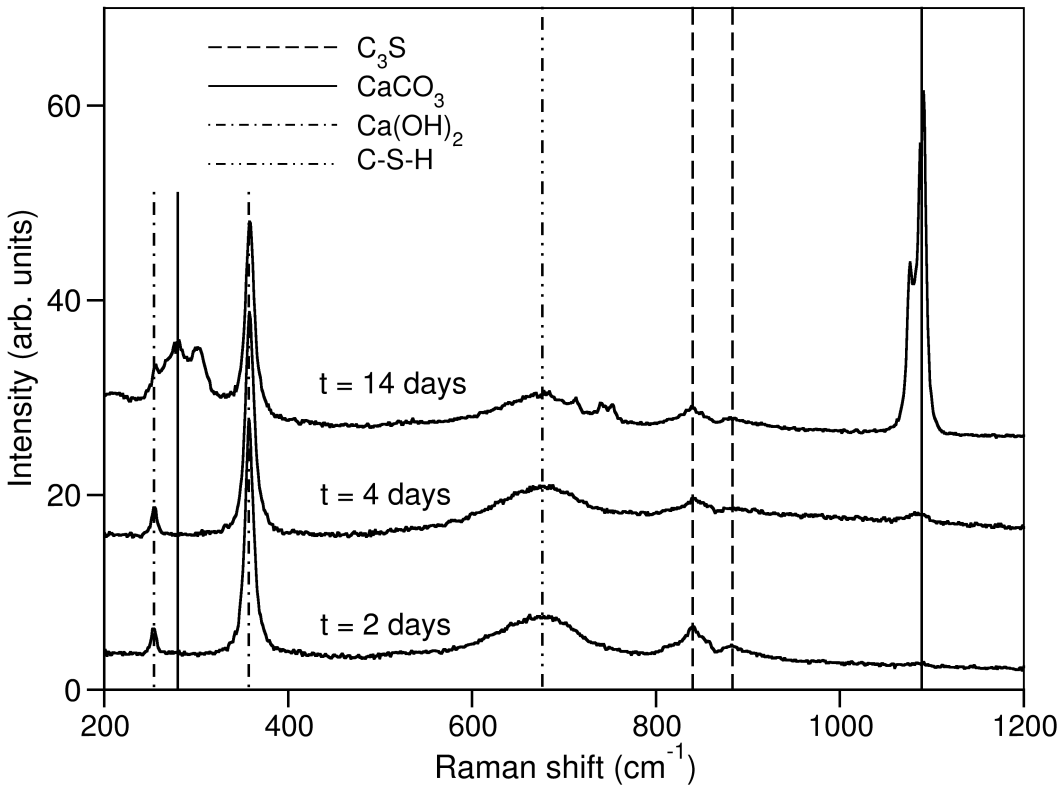

Figure S.9 Preservation of the water-to-solid ratio of 0.5 over longer periods of times (2 to 4 days) prevents the formation of calcium carbonate (highlighted by the absence of the $CaCO_3$ Raman band), and favors the formation of the expected hydration products, $Ca(OH)_2$ and C-S-H (characterized by the bands at 255 and 360 cm^{-1} for the former, and by the broad shoulder at 674 cm^{-1} for the latter [14]). The significant carbonate formation after 14 days coexists with the presence of the hydration products, $Ca(OH)_2$ and C-S-H, suggesting that the origin of $CaCO_3$ at later hydration stages, is not the result of evaporation, but rather by reaction of the hydration products with CO_2 [5].

S.8 Raman spectroscopy

Micro-Raman spectra were acquired (JY Horiba LabRam HR800 spectrometer in backscattering configuration), with an excitation line provided by a HeNe laser (excitation wavelength: 632.8 nm) through a confocal microscope (Olympus BX41, 100X objective). A 600 spectral grating was used, providing a spectral resolution of $\sim$1.2 cm^{-1}. Sample manipulation was carried out with a micro-mechanical stage to obtain high-lateral control over the position of the laser spot (diameter $\sim$ 800 nm for the excitation wavelength used, 632 nm). For each point of interest, five Raman spectra were acquired (with acquisition of five seconds each) and averaged. Because of the absence of fluorescence or any background, the analysis did not require special background subtraction.

In a typical experiment, picoliter droplets were grown on cover slips over glass slides. These slides were then transferred within few minutes from the synthesis under the optical microscope in the Raman spectrometer. Several droplets were selected and their location tracked (with accuracy of 100 nm), so the evolution of the same droplet could be at predetermined time steps. Raman spectroscopy measurements on hydrated pastes (prepared as described in Section S.5) were acquired on pastes transferred from the environmentally controlled environment to a glass slide. In light of the crucial role played by evaporation in the formation of carbonate species, both the surface of the cement paste (which is more susceptible to evaporation than its bulk) and the bulk itself were used for the measurement.

To minimize the contribution of evaporation induced by the excitation laser, a filter was used to reduce the power density to the sample to about 5 $\mu W/\mu m^2$. To ensure these acquisition parameters would induce no evaporation, several acquisitions were carried out in the same location with known hydration conditions. No detectable difference among the spectra were observed. For the experiments where laser-induced heating and evaporation was sought to accelerate carbonation, no filter was used and the maximum power density to the sample was approximately 50 $\mu W/\mu m^2$. Under these conditions, we observed a rapid formation of calcium carbonate, almost in real time (within the shortest time acquisition for individual spectra, 1 s).

Attribution of vibrational modes in the Raman spectra of pure and hydrated tricalcium silicate as well as calcium carbonates and calcium hydroxide were obtained from well-established literature [14–19].

References

1. Lamprecht, M., Sabatini, D., Carpenter, A. *et al.* Cellprofiler: free, versatile software for automated biological image analysis. *Biotechniques* **42**, 71 (2007).

2. Garrault, S., Finot, E., Lesniewska, E. & Nonat, A. Study of CSH growth on C_3S surface during its early hydration. *Materials and structures* **38**, 435–442 (2005).

3. Severinghaus, J., Broecker, W., Dempster, W., MacCallum, T. & Wahlen, M. Oxygen loss in biosphere 2. *EOS Transaction - AGU* **75**, 33–40 (1994).

4. Young, J., Berger, R. & Breese, J. Accelerated curing of compacted calcium silicate mortars on exposure to CO_2. *J. Am. Ceram. Soc.* **57**, 394–397 (1974).

5. Rostami, V., Shao, Y., Boyd, A. & He, Z. Microstructure of cement paste subject to early carbonation curing. *Cement and Concrete Research* **42**, 186 (2012).

6. Reuter, D., Gerth, G. & Kirschner, J. *Surface Diffusion*, vol. 360, 489 (Plenum Press, 1997).

7. Ferralis, N., El Gabaly, F., Schmid, A., Maboudian, R. & Carraro, C. Real-time observation of reactive spreading of gold on silicon. *Phys. Rev. Lett.* **103**, 256102 (2009).

8. Rasband, W. ImageJ. http://imagej.nih.gov/ij/ (1997-2013).

9. Schneider, C., Rasband, W. & Eliceiri, K. NIH image to ImageJ: 25 years of image analysis. *Nature Methods* **9**, 671–675 (2012).

10. Juenger, M., Monteiro, P., Gartner, E. & Denbeaux, G. A soft x-ray microscope investigation into the effects of calcium chloride on tricalcium silicate hydration. *Cement and Concrete Research* **35**, 19–25 (2005).

11. Bullard, J. *et al.* Mechanisms of cement hydration. *Cement and Concrete Research* **41**, 1208–1223 (2011).

12. Thomas, J. *et al.* Modeling and simulation of cement hydration kinetics and microstructure development. *Cement and Concrete Research* **41**, 1257–1278 (2011).

13. Haselbach, L. Potential for carbon dioxide absorption in concrete. *Journal of Environmental Engineering* **135**, 465–472 (2009).

14. Black, L. Raman spectroscopy of cementitious materials. *Spectroscopic Properties of Inorganic and Organometallic Compounds: Materials and Applications* **40**, 72–127 (2009).

15. Kirkpatrick, R., Yarger, J., McMillan, P., Ping, Y. & Cong, X. Raman spectroscopy of CSH, tobermorite, and jennite. *Advanced Cement Based Materials* **5**, 93–99 (1997).

16. Padanyi, Z. The Raman spectrum of $Ca(OH)_2$. *Solid State Communications* **8**, 541–543 (1970).

17. Martínez-Ramírez, S. & Fernández-Carrasco, L. *Raman spectroscopy: application to cementitious systems* (Nova Science Publishers, 2011).

18. Potgieter-Vermaak, S., Potgieter, J. & Van Grieken, R. The application of Raman spectrometry to investigate and characterize cement, part I: A review. *Cement and concrete research* **36**, 656–662 (2006).

19. Downs, R. The RRUFF project: an integrated study of the chemistry, crystallography, raman and infrared spectroscopy of minerals. *9th General Meeting of the International Mineralogical Association* **O03-13** (2006). URL `http://rruff.info/`.